PROCEEDINGS OF SPIE

SPIEDigitalLibrary.org/conference-proceedings-of-spie

Photoinhibited superresolution lithography: overcoming chemical blur

Darren L. Forman, Robert R. McLeod

Darren L. Forman, Robert R. McLeod, "Photoinhibited superresolution lithography: overcoming chemical blur," Proc. SPIE 9049, Alternative Lithographic Technologies VI, 90491W (28 March 2014); doi: 10.1117/12.2063254

SPIE.

Event: SPIE Advanced Lithography, 2014, San Jose, California, United States

Downloaded From: https://www.spiedigitallibrary.org/conference-proceedings-of-spie on 6/16/2018 Terms of Use: https://www.spiedigitallibrary.org/terms-of-use

Photoinhibited superresolution lithography: overcoming chemical blur

Darren L. Forman and Robert R. McLeod
University of Colorado at Boulder

ABSTRACT

Photoinhibited superresolution (PInSR) lithography is a two-color, one-photon scheme that promises high throughput far-field patterning at deep subwavelength scales. Previous work has shown that the technique is susceptible to blurring from active species diffusion, an issue which we have recently overcome with the use of a low-diffusivity methacrylate resist. Here we present our first clear demonstration of superresolution, showing feature spacing 3x better than the 0.2 NA diffraction limit.

Keywords: Superresolution, STED, lithography, photoinhibition

1. INTRODUCTION

Photopolymerization, initiated by the absorption of incident light and propagated by the chain-reaction of reactive centers, is a fast and efficient means for creating patterned material changes required for lithography and data storage. The minimum dense-pattern feature size, or critical dimension (CD) is traditionally defined by the Abbe diffraction limit, $CD = k_1\lambda/NA$, where λ is wavelength, NA is numerical aperture and k_1 is an engineering parameter with a fundamental lower limit of 0.25 for a single exposure.[1] With the advent of immersion deep UV lithography, the approximate resolution limits of conventional optical patterning appear to have been reached. Significantly finer single-exposure patterning requires shorter wavelength radiation, where there remain technically significant challenges in sources and materials.

With these obstacles in mind, several methods have been proposed for patterning that is unconstrained by the diffraction limit. One family of them,[2–4] including the one dealt with here, are inspired by the two color, two beam superresolution concept utilized by stimulated-emission depletion (STED) microscopy.[5] A significant challenge with some of these techniques is the degree to which the material response to one color of light can be inhibited by the other color; absorption contrast limitations in photochromics,[2] and complexities in initiator de-excitation,[6] are examples of this. With photoinhibited superresolution (PInSR), however, an inhibition response has been shown that would seem strong enough to demonstrate patterning well below the diffraction limit.[7] But with this last method, as we recently showed,[8] diffusion of active species can result in serious blurring and prevent superresolved patterning.

Another group, using a very similar technique, has recently claimed dramatically superresolved results [9] that deserve attention. But a number of factors, especially radical diffusion[8] and the strong chain-transfer / termination effect of the photoinhibitor TED on acrylates,[10] lead us to wonder if the results are actually enabled by other physics. For the sake of simplicity, we restrict our attention here to the scheme first presented in [4].

This paper revisits [8] to present our current understanding of PInSR fundamentals and reveal the limitations of previously discussed materials, and goes on to present results from a new material formulated to address those limitations.

2. EXPERIMENTAL

2.1 Optics and Mechanics

An Omicron diode laser emitting a CW beam at λ = 473 nm was used as the initiating source. A Coherent Innova 300C Argon-ion laser emitting a CW beam at λ = 364 nm was used as the inhibiting source. Beam powers listed elsewhere in this work are measured at the entrance to the objective lens.

A custom dichroic mirror, designed to reflect blue and transmit UV, was used to combine the two beams and direct them into the objective lens. Two Zeiss Ultrafluar microscope objectives were used in this work, a 100x 1.2 NA 365 glycerol-immersion lens and a 10x 0.2 NA dry lens. Crucially, both lenses are well-corrected in both the UV and visible

Further author information: (Send correspondence to Robert R. McLeod)
E-mail: Robert.Mcleod@colorado.edu

Alternative Lithographic Technologies VI, edited by Douglas J. Resnick, Christopher Bencher, Proc. of SPIE
Vol. 9049, 90491W · © 2014 SPIE · CCC code: 0277-786X/14/$18 · doi: 10.1117/12.2063254

Downloaded From: https://www.spiedigitallibrary.org/conference-proceedings-of-spie on 6/16/2018 Terms of Use: https://www.spiedigitallibrary.org/terms-of-use

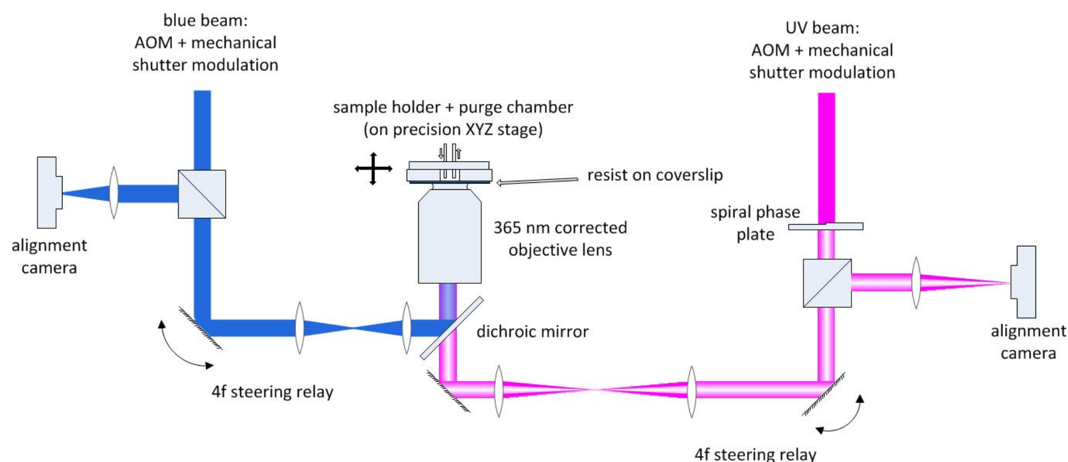

Figure 1. Optical schematic: writing and inhibiting beams pass through separate spatial filters, shutters, waveplates and steering relays, with the inhibiting beam also passing through a spiral phase plate to achieve conversion to the GL10 mode. The beams are combined with a dichroic mirror, and directed into an objective lens that focuses them onto the sample. A motorized XYZ stage is used to raster-scan the sample above the modulated beams.

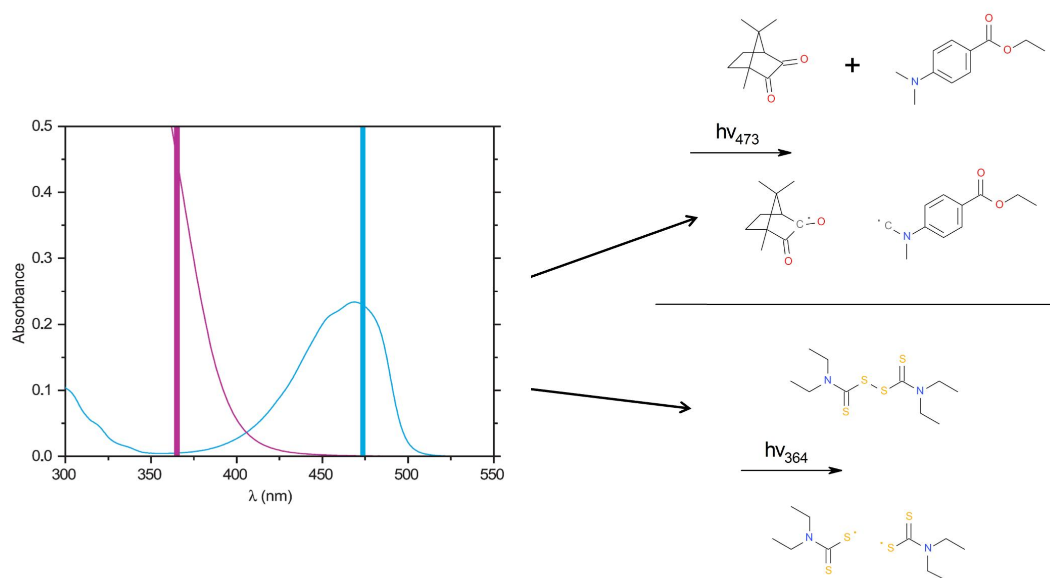

Figure 2. Photochemistry schematic: upon absorbing $\lambda = 473$ nm blue light, camphorquinone (CQ) reacts with a tertiary amine (EDAB) to form a chain-initiating aminoalkyl radical. Upon absorbing $\lambda = 364$ nm UV light, tetraethylthiuram disulfide (TED) undergoes homolytic fission to form 2 chain-terminating dithiocarbamyl (DTC) radicals.

bands. Standard visible and UV optics were used to attenuate, spatially filter and steer the beams, and to create circular polarization in both beams at the back aperture of the objective. A spiral phase plate from RPC Photonics was used when a donut-shaped UV beam was needed, otherwise it was omitted.

Each beam was independently modulated with a Vincent Associates mechanical shutter, VS25 for UV and LS2 for blue. The shutter driver was signaled by a digital delay generator (DG-535, Stanford Research).

Axial alignment of the two-beam focus was measured by independently monitoring the blue and UV confocal reflections from a glass/air interface. To compensate for the small axial chromatic shift caused by the objective lens, the blue beam was slightly decollimated. Transverse alignment was measured at 1.2 NA by imaging reflections from 100 nm gold nanoparticles (Sigma Aldrich) deposited on a coverslip surface and embedded in polymerized triethylene glycol dimethacrylate (Sigma Aldrich), and at 0.2 NA by measuring beam transmission through a pinhole in gold that had been sputtered on a coverslip.

Downloaded From: https://www.spiedigitallibrary.org/conference-proceedings-of-spie on 6/16/2018 Terms of Use: https://www.spiedigitallibrary.org/terms-of-use

The sample was positioned by Newport XMS-series stages in XY and a GTS30V stage in Z, and was driven by a Newport XPS controller.

2.2 Materials

Chemicals were used as received from the supplier, without further purification apart from 0.2 μm particle filtering. Number 1 coverslips (VWR) were used as substrates and were cleaned by a 30 second dip in room-temperature Nanostrip (Cyantek), rinsed in DI-water and dried under a N2 stream. For the material evaluated in Fig. 3: On one side of the coverslips, a thin layer of gold was sputter deposited to yield a reflective interface with a transmission of 60% at λ = 473 nm. A spinnable adhesion-promoting resist was made with 1 wt% 2,4,6-trimethylbenzoyldiphenylphosphine oxide (Lucerin TPO, BASF) in urethane dimethacrylate (Esstech), combined 1:1 with cyclohexanone (Sigma Aldrich) and filtered. The resist was then spin-coated at 2000 rpm for 45 seconds onto the gold side of the coverslip, placed under a purge of research-grade nitrogen (Airgas), and extensively cured with a UV mercury lamp (Efos Ultracure 100ss Plus) to yield a hard, cross-linked polymer film. The PInSR resin itself was prepared from ethoxylated bisphenol-A dimethacrylate (E2BADMA or SR348, Sartomer), with 1 wt% camphorquinone (CQ), 0.5 wt% ethyl 4-(dimethylamino)benzoate (EDAB) and 3 wt% tetraethylthiuram-disulfide (TED) added to the resin (all from Sigma Alrich). For the materials evaluated in Fig. 4 and Fig. 5: The resin was prepared as before, but with 0.1% CQ, Isophorone Urethane Dimethacrylate (UDMA-IPDI, Esstech) instead of E2BADMA and with 5 wt% glass adhesion promoter (PL-2212, Esstech).

2.3 Sample preparation and exposure

Resin samples made from E2BADMA were laminated without a spacer between the coverslip and nonstick-slide (functionalized with a fluorinated silane coupling-agent, Gelest), to create a layer estimated to be no more than a few microns thick. This configuration has the advantage of limiting the axial extent of polymerized features and serves as a barrier from atmospheric oxygen, a strong radical inhibitor. Once prepared, samples were mounted on the stage and cantilevered over the upward-facing objective lens. The sample was then lowered into the immersion medium and the gold layer near the substrate/resin interface was located by confocal reflection. After mapping the z-axis (vertical direction) of the exposure area perimeter, spot exposures focused on the substrate/resin interface were raster-scanned by a combination of xyz stage movements and shutter modulations.

Resin made from UDMA-IPDI was spin-coated from cyclohexanone onto cleaned coverslips to form a ~ 1 μm thick film. The samples were then mounted onto a nitrogen-purged sample holder and exposed as above. To prevent CQ and EDAB evaporation, the nitrogen flow first passed through a flask containing a stirred solution of CQ and EDAB in vacuum pump oil.

2.4 Sample development

Exposed samples were carefully delaminated using a razor blade to wedge the coverslip from the microscope slide. The coverslip was then gently rinsed for 30 seconds in cyclohexanone (Sigma Aldrich) then for 30 seconds in spectro-grade methanol (Burdick and Jackson) before being dried under a gentle air stream.

2.5 Characterization

Polymer dot arrays were inspected with a Olympus AX70 microscope operating in darkfield reflection mode, using 0.5-0.9 NA air objectives. Electron microscope images of gold-coated polymer features were obtained with a JSM-7401F field-emission SEM at an accelerating potential of 5 kV.

3. RESULTS AND DISCUSSION

Photoinhibited radical polymerization is likely possible in a variety of systems, with our own work indicating most methacrylate-based resists and resins can be photoinitiated with the CQ / EDAB system and photoinhibited with TED. With focused spot exposures, we confirmed in various methacrylate resins that knob-shaped polymer dots[8] may be formed with dimensions matching or even smaller than the full-width half-max (FWHM) of the focused blue Gaussian spot. But in this regime polymer dot size is observed to be an approximately linear function of exposure time, meaning that over-exposures can result in gelled dots with significantly larger diameters. Considering the exponential decrease of the PSF with transverse distance, this result is somewhat surprising and may indicate significant out-diffusion of radicals. But even

Downloaded From: https://www.spiedigitallibrary.org/conference-proceedings-of-spie on 6/16/2018 Terms of Use: https://www.spiedigitallibrary.org/terms-of-use

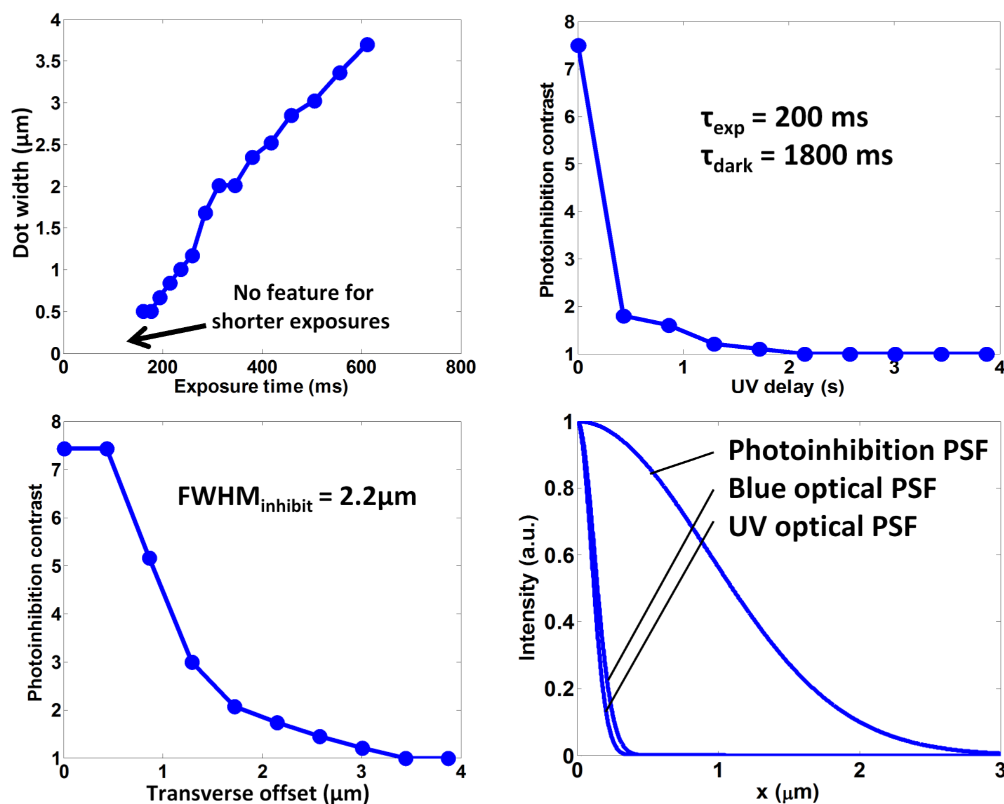

Figure 3. Measurement of PInSR dynamics and the diffusion-blurring problem. Top left: The polymer dot width is an approximately linear function of exposure time (P_B = 4.1 μW). Top right: Blue and UV exposures are staggered in time to estimate the lower limit of the dark polymerization interval. For small gelled features resulting from a 200 ms blue exposure, the photoinhibition effect is observed as long as 2 seconds later (P_B = 4.1 μW, P_{UV} = 130 μW, t_{exp} = 100-600 ms). Bottom left: The photoinhibition effect of the UV beam is measured as a function of spot offset. Relative to spot centroid alignment, photoinhibition contrast falls to half for a spot offset of 1.1 μm (P_B = 4.1 μW, P_{UV} = 130 μW, t_{exp} = 100-600 ms). Bottom right: A comparison of the optical PSFs and the measured photoinhibition PSF. All PSFs are taken to be Gaussian, scaled appropriately to the measured FHWM.

so, the achievement of dots with dimensions matching the writing spot suggests that the confinement of carbon-centered radicals (which initiate chains and propagate chain-growth) is sufficient to evaluate photoinhibited superresultion (PInSR).

The photoinhibition effect may readily be observed by removing the phase plate, superimposing a Gaussian-shaped λ = 364 nm UV spot on the blue spot, and adjusting the UV intensity to cause an increased exposure time required to gel dots in the sample.[7]

A similar photoinhibition effect is also apparent when the spiral phase plate is replaced and the dark center of donut-shaped UV spot is aligned with the bright center of the blue spot. By comparing the dimensions of dots fabricated without the inhibiting donut beam to those fabricated with it on, we expect to observe the enhanced polymer confinement required for superresolution patterning. What we actually observe, however, is an unchanged polymer confinement; the smallest dots fabricated with the superimposed Gaussian-blue and donut-UV spots are the same size as the smallest dots fabricated with Gaussian-blue spots alone [8], which is rather disappointing. The increased exposure time-to-gel associated with the UV photoinhibition is observed, but the effect appears to be equivalent to lowering the power of a blue-only writing beam; instead of enhancing confinement of polymer dots, the addition of the UV spot reduces polymerization efficiency.

With this observation, we undertook an investigation into the fundamental spatial and temporal characteristics of the PInSR system.[8] Since we were not able to observe features significantly smaller than 100 nm fabricated from the resist described in [7], we decided to investigate the material system for which good results have been reported: an ethoxylated (2) bisphenol-A dimethacrylate (E2BADMA) resin used by Gu et al. to achieve 40 nm dots.[11] The resin has a viscosity η = 1000 cP @ 25 C, and contains the same photochemistry (CQ, EDAB and TED) as the original work.[4] With respect to the

Downloaded From: https://www.spiedigitallibrary.org/conference-proceedings-of-spie on 6/16/2018 Terms of Use: https://www.spiedigitallibrary.org/terms-of-use

optical system, the measured relative position and profile of the beams are reasonably well characterized; spot dimensions as measured with gold dots are $FWHM_B$ = 290 nm and $FWHM_{UV}$ = 240 nm, with spot alignments better than 50 nm. With the spiral phase plate removed, the superimposed Gaussian-UV and Gaussian-blue spots are used to write a column of dots where the exposure time increases along the column. The next column is the same but now the spots have been transversely offset. The third column has twice that offset, and the forth column three times etc. The photoinhbition effect of the UV spot diminishes with increased offset with the blue spot, but much more slowly than expected; a spot centroid transverse offset of 1.1 μm is required to decrease the photoinhibition contrast by half (BL, Fig.3). Here we define photoinhibition contrast (PIC) as PIC = $\tau_{exp(B+UV)}/\tau_{exp(B)}$, where $\tau_{exp(B)}$ is the minimum exposure time to gel the dot with the inhibition beam off, and $\tau_{exp(B+UV)}$ is the minimum exposure time to gel the dot with the Gaussian inhibition beam on. This wide radius of measured inhibition is an order of magnitude larger than the optical spot that generates it, indicating that the photoinhibition effect has spread significantly beyond the extent of the UV PSF in the time scale of polymer gelation. This in turn suggests that radical diffusion rate is too fast relative to the polymerization rate for enhanced polymerization confinement at this spatial scale.

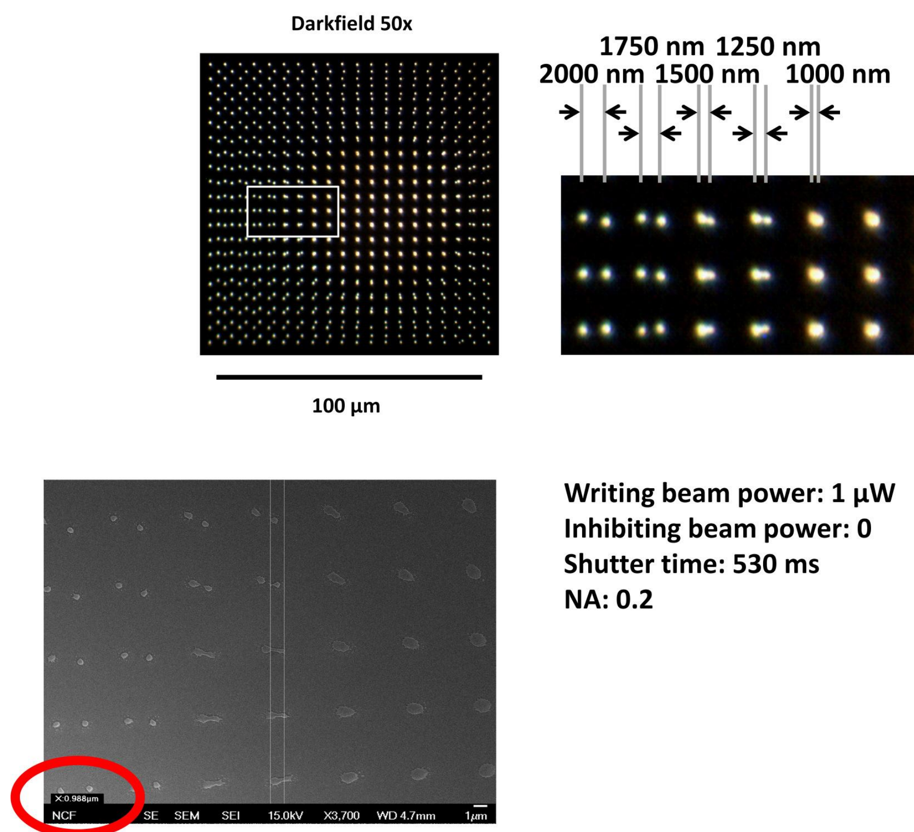

Figure 4. Control pattern (inhibiting beam off) written at 0.2 NA in UDMA-IPDI resin. Top: 0.8 NA optical darkfield micrograph with zoomed inset, bottom: FE-SEM images of same pattern. The Sparrow resolution criterion is met at $\sim$1000 nm dot spacing.

From the real-time FTIR studies of photopolymerization by Decker[12] of short exposures to intense laser beams, we see that the majority of the conversion may occur after the exposure, over longer intervals in the dark (so-called dark cure or dark polymerization). To obtain an estimate of the minimum time-to-gel, we use a variable delay of the UV exposure relative to the blue exposure. With sufficient UV delay, the photoinhibition effect is not observed; we then use this delay as an estimate of the minimum time to gel. Relative to simultaneous exposures (no UV delay) the photoinhibition contrast is observed to fall by 75% within 0.5 seconds, the minimum delay implemented. With a delay of more than 2 seconds, no change in photoinhibition is observed. Since no photoinhibition effect is possible in the dot after it gels, we take 2 seconds as a minimum time to gel for the given exposure.

To achieve well-defined superresolved polymer features, the photoinhibitor concentration must retain the profile of the

Downloaded From: https://www.spiedigitallibrary.org/conference-proceedings-of-spie on 6/16/2018 Terms of Use: https://www.spiedigitallibrary.org/terms-of-use

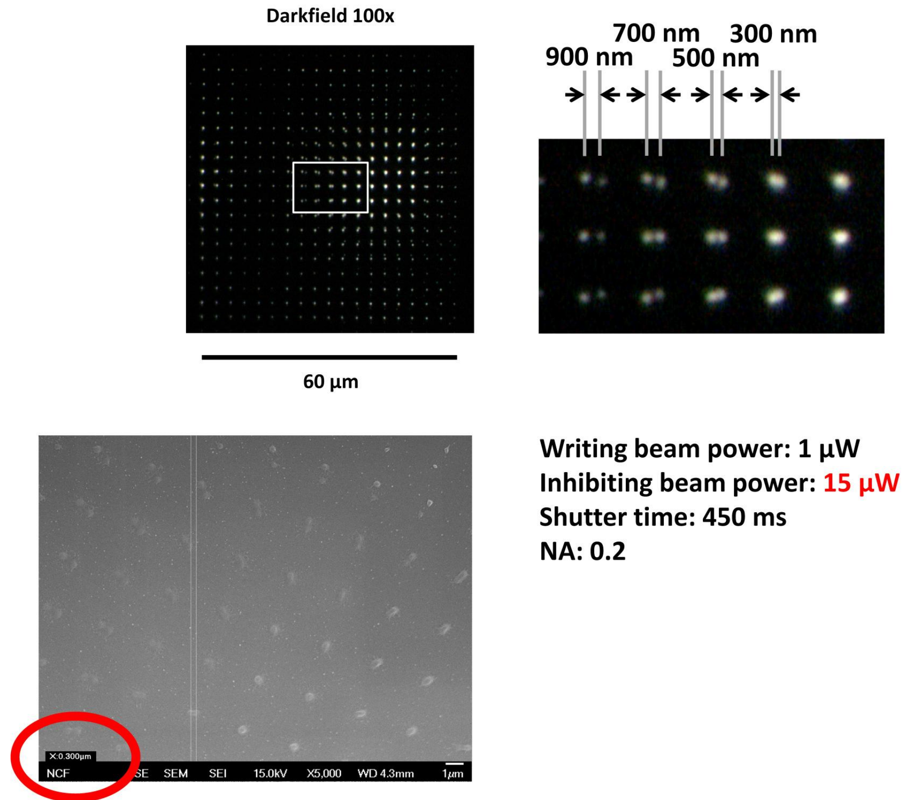

Figure 5. Test pattern (inhibiting beam on) written with parameters otherwise same as above. Top: 0.8 NA optical darkfield micrograph with zoomed inset, bottom: FE-SEM images of same pattern. Sparrow resolution criterion is met at ∼300 nm dot spacing. Darker regions of top dot array may be caused by slight underexposure during writing.

UV optical spot for at least the gelation time interval. We must thus compare the measured gelation time to the DTC radical diffusion time into the dark UV null. Fig.3 BL indicates diffusion of DTC radicals sufficient to reduce contrast by 50% over a distance of approximately 1 micron in the gelation time, indicating that the diffusion time across the approximately 100 nm PSF may be a factor of 100 smaller than the gelation time. As direct measurement of the DTC radical diffusivity is difficult, we substitute the DTC radical with a fluorescent molecule of similar size and measure its diffusivity via fluorescence-recovery-after-photobleaching (FRAP).[13]

Adding 7-mercapto-4-methylcoumarin to the monomer causes visible fluorescence to occur under a UV lamp, which is not observed in the neat monomer. Using a 0.25 NA microscope objective, thin laminated samples are observed to fluoresce and then quickly bleach under focused $\lambda = 364$ nm light. A camera placed behind a UV filter is used to measure fluorescence intensity and the bleaching process. After using an intense UV beam to quickly bleach the spot in < 0.5 seconds with bleaching parameter K of approximately 10,[13] half the fluorescence intensity returns after 5.0 seconds.

Using the equation from [13], $D = \gamma_D w^2/4\tau_{1/2}$, we find D to be 0.26 $\mu m^2/s$, which agrees closely with the value used in [14]. Considering that the hole radius of the UV donut is approximately 100 nm (using the 1.2 NA writing lens), radical in-diffusion time may be estimated using the same analysis. For this, we assume a circular hole of w = 100 nm and γ_D = 0.88.[13] The estimated diffusion time $\tau_{1/2\ DTC}$ taken for DTC radicals to halfway fill-in the hole is 8.5 ms, 230x faster than the 2 second estimated polymerization and consistent with the order-100x factor estimated earlier from spot offsets. Given this material with those parameters known a-priori, we would not have expected to achieve enhanced submicron confinement through patterned photoinhibition.

After this discovery, we decided to slow diffusion-induced blurring in two ways: formulating the resin for significantly lower small-molecule diffusivity and reducing the numerical aperture. Isophorone Urethane Dimethacrylate is known to have a high viscosity,[15] which we measured to be $\eta = 500{,}000$ cP at room temperature. We attempted FRAP measurements in the resin with 7-mercapto-4-methylcoumarin, and while thermal drift in sample positioning ultimately prevented the

Downloaded From: https://www.spiedigitallibrary.org/conference-proceedings-of-spie on 6/16/2018 Terms of Use: https://www.spiedigitallibrary.org/terms-of-use

observation of fluorescence recovery, we were able to estimate that the diffusivity D $< 0.001\ \mu m^2/s$. This is at least a factor ~ 240 reduction in diffusivity compared to the E2BADMA resin. Together with the factor ~ 36 reduction in relative diffusion achieved by lowering the NA from 1.2 to 0.2, we expect a net slowing of diffusion by factor of more than ~ 8500.

Figures 4 and 5 show that these measures successfully address the earlier limitations. For the control experiment in Fig. 4, two polymer dot grids were written in sequence. The first had a square spacing of 5.0 μm and the second of 5.25 μm. The Sparrow diffraction[16] limit is observed for dot spacings of $\sim$1000 nm, as expected for λ = 473 nm light at 0.2 NA. For the test experiment in Fig. 5, the first dot grid had a square spacing of 3.0 μm and the second of 3.2 μm. Here, the Sparrow diffraction limit is observed for dot spacings of $\sim$300 nm, thus demonstrating a 3-fold improvement in resolution.

4. CONCLUSIONS

We have found that enhanced pattern confinement in PInSR depends strongly on the mobility of active species. Fast blurring of photo-generated inhibitor is seen in E2BADMA relative to the polymerization timescale, which most likely explains our inability to achieve superresolution in that material via PInSR. To address the issue, we formulated a new PInSR resin from a highly viscous monomer with significantly lower mobility. We also used low-NA optics to further slow diffusion relative to the spot size. This results in a demonstrated 3-fold improvement in resolution beyond the diffraction limit.

ACKNOWLEDGMENTS

The authors wish to acknowledge funding from NSF CAREER award ECCS 0954202 and a gift from the Oracle Corporation. DF has been supported by the DoD NDSEG and NSF COSI:IGERT programs.

REFERENCES

1. Pease, R. F. and Chou, S. Y., "Lithography and other patterning techniques for future electronics," *Proceedings of the IEEE* **96**(2), 248–270 (2008).
2. Andrew, T. L., Tsai, H.-Y., and Menon, R., "Confining light to deep subwavelength dimensions to enable optical nanopatterning," *Science* **324**(5929), 917–921 (2009).
3. Linjie Li, R. R. G. E. G. H. H. and Fourkas, J. T., "Achieving lambda/20 resolution by one-color initiation and deactivation of polymerization," *Science* **324**(5929), 3 (2009).
4. Scott, T. F., Kowalski, B. A., Sullivan, A. C., Bowman, C. N., and McLeod, R. R., "Two-color single-photon photoinitiation and photoinhibition for subdiffraction photolithography," *Science* **324**(5929), 913–917 (2009).
5. Hell, S. W. and Wichmann, J., "Breaking the diffraction resolution limit by stimulated emission: stimulated-emission-depletion fluorescence microscopy," *Opt. Lett.* **19**(11), 780–782 (1994).
6. Stocker, M. P. and Fourkas, J. T., "Elucidating the kinetics and mechanism of rapid lithography," in [*SPIE MOEMS-MEMS*], 824902–824902–7, International Society for Optics and Photonics (2012).
7. Forman, D. L., Heuvelman, G. L., and McLeod, R. R., "Materials development for photo-inhibited super-resolution (pinsr) lithography," in [*SPIE MOEMS-MEMS*], 824904–824904–9, International Society for Optics and Photonics (2012).
8. Forman, D. L., Cole, M. C., and McLeod, R. R., "Radical diffusion limits to photoinhibited superresolution lithography," *Physical Chemistry Chemical Physics* **15**(36), 14862–14867 (2013).
9. Gan, Z., Cao, Y., Evans, R. A., and Gu, M., "Three-dimensional deep sub-diffraction optical beam lithography with 9 nm feature size," *Nature communications* **4** (2013).
10. Kilambi, H., Reddy, S. K., and Bowman, C. N., "Kinetic and mechanistic studies of photopolymerizations of acrylates in the presence of iniferters," *Macromolecules* **40**(17), 6131–6135 (2007).
11. Cao, Y. Y., Gan, Z. S., Jia, B. H., Evans, R. A., and Gu, M., "High-photosensitive resin for super-resolution direct-laser-writing based on photoinhibited polymerization," *Optics Express* **19**(20), 19486–19494 (2011).
12. Decker, C. and Moussa, K., "Real-time kinetic study of laser-induced polymerization," *Macromolecules* **22**(12), 4455–4462 (1989).
13. Axelrod, D., Koppel, D., Schlessinger, J., Elson, E., and Webb, W., "Mobility measurement by analysis of fluorescence photobleaching recovery kinetics," *Biophysical journal* **16**(9), 1055 (1976).

Downloaded From: https://www.spiedigitallibrary.org/conference-proceedings-of-spie on 6/16/2018 Terms of Use: https://www.spiedigitallibrary.org/terms-of-use

14. Gan, Z. S., Cao, Y. Y., Jia, B. H., and Gu, M., “Dynamic modeling of superresolution photoinduced-inhibition nanolithography,” *Optics Express* **20**(15), 16871–16879 (2012).
15. Atai, M., Ahmadi, M., Babanzadeh, S., and Watts, D. C., “Synthesis, characterization, shrinkage and curing kinetics of a new low-shrinkage urethane dimethacrylate monomer for dental applications,” *Dental Materials* **23**(8), 1030–1041 (2007).
16. Sparrow, C. M., “On spectroscopic resolving power,” *The Astrophysical Journal* **44**, 76 (1916).

Downloaded From: https://www.spiedigitallibrary.org/conference-proceedings-of-spie on 6/16/2018 Terms of Use: https://www.spiedigitallibrary.org/terms-of-use